Heritage Science

RESEARCH

Open Access

Laser-based techniques for the non-invasive characterisation of grisaille paints on stained-glass windows

Carla Machado[1,2*], Mohamed Oujja[3], Luís Cerqueira Alves[4], Marina Martínez-Weinbaum[3], Laura Maestro-Guijarro[3], Paula María Carmona-Quiroga[3], Marta Castillejo[3], Márcia Vilarigues[1,2] and Teresa Palomar[2,5]

Abstract

Grisaille was the first paint applied on stained-glass panels, used in Europe since the twelfth century. Historical written sources described the use of iron and copper together with a high lead-silica base glass in the grisailles production. This project aims to study the evolution of the grisaille paint composition throughout time and the changes in the raw materials used in their production using non-destructive and non-invasive techniques. To achieve this objective, 23 grisaille samples dated from the 13th to the twentieth centuries from nine different countries (Portugal, Poland, United Kingdom, Sweden, Norway, Belgium, Low Countries, Germany, and France) were studied by means of micro particle-induced X-ray emission (μ-PIXE), micro energy dispersive X-ray fluorescence (μ-EDXRF), laser-induced breakdown spectroscopy (LIBS), laser-induced fluorescence (LIF), non-linear optical microscopy (NLOM) in the modality of multiphoton excitation fluorescence (MPEF) and optical microscopy (OM). The results showed that it was possible to identify compositional differences and patterns throughout the samples when compared with literature results. The preference for using copper in central and south-central European countries and the addition of new compounds (CoO, Cr_2O_3, MnO) as colouring agents since the nineteenth century was verified. The LIBS analyses allow the identification of boron on two samples, confirming the change of base glass components since the seventeenth century. The NLOM-MPEF showed the capability of this technique to measure the grisaille paint layers' thickness. This non-invasive multi-analytical and complementary approach proves itself efficient in identifying changes in the grisaille's composition throughout time, which can be interpreted as changes in the raw materials and manufacture used in the production of these paint materials.

Keywords Stained-glass windows, Grisaille, Multi-analytical characterisation, Thickness measurements, Laser spectroscopies, Non-linear optical microscopy

Introduction

Grisailles are dark (black/brown) vitreous paints used in the production of stained-glass panels. Generally, grisailles are employed in the creation of outlines (*grisaille à contourner*) and shadows (*grisaille à modéler*) [1, 2]. These are the oldest painting materials as well as the most used in stained-glass windows from medieval times until today [2, 3]. Written sources, such as the twelfth century *De Diversis Artibus* by Theophilus [4], describe the production of grisailles by mixing metals oxides, usually iron and/or copper oxides (Fe_2O_3 and/or CuO), as colouring agents, with a grounded lead-based glass ($PbO\text{-}SiO_2$), responsible for the adhesion of the grisaille paint to the glass substrate [1]. These paints are usually mixed with vehicles (water, vinegar, wine, etc.) and temporary binding agents (gum arabic), applied on the glass

*Correspondence:
Carla Machado
cf.machado@campus.fct.unl.pt
Full list of author information is available at the end of the article

support and fired at 650–700 °C [1, 3]. After the firing of the grisaille, the base glass will soften and fix to the glass support, leaving a thin heterogeneous layer of colourless glass with the colouring agents grains (metal oxides) dispersed [1, 2, 5].

The heterogeneity characteristic of these paint layers can challenge the accuracy of chemical composition characterisation. [2, 3, 6, 7] Stained-glass fragments with grisaille paint are also particularly important for conservators and restorers as they maintain the original paint, usually located in the middle of the fragment, complicating the sampling [3].

The study and interest in this material has increased all over the years. Different techniques analyse historical grisaille samples and their chemical composition [3]. The most common techniques are laboratory-based ones such as scanning electron microscopy coupled with energy-dispersive spectrometry (SEM–EDS), X-ray fluorescence spectrometry (XRF) and X-ray diffraction (XRD) [3]. The first two techniques (SEM–EDS and XRF) allow the semi or quantitative chemical composition [8–11], and XRD permits the identification of crystalline compounds [8, 10, 12, 13], which are usually the colouring agents. Even though using these techniques could be applied in a minimally invasive way on the sample surface, they are sensitive to the irregularities and the weathered products present on the paint layers. This makes it difficult to accurately analyse the grisaille layers. It is necessary to prepare the samples in resin and to analyse them in cross-sections, destroying the samples from valuable and unique stained-glass windows. Furthermore, techniques such as portable XRF have difficulty detecting low Z elements (boron, sodium and magnesium), mainly in samples with high variety of Z elements.

For example, Pradell et al. [13] identified boron in samples from the seventeenth century onwards using the destructive technique of laser ablation inductively coupled plasma mass spectroscopy (LA-ICP-MS). The boron consists of the probable addition of borax ($Na_2B_4O_7.10H_2O$) during the grisaille production since that time, providing key information for understanding technological changes in grisaille production through time. The addition of borax can reduce the firing temperature of the grisailles, which can raise questions on why the need for lower temperature: (1) changes in the composition of the base glasses used in grisailles manufacturing, or (2) changes in the composition of the support glasses, leading them to not support higher temperatures without deforming.

Therefore, looking for non-invasive, micro-destructive, and complementary techniques, it is important to gather more in-depth information about the studied materials. Different non-invasive or micro-invasive techniques have been used and tested to characterise and study stained-glass windows and glass objects [14–16]. Laser-based techniques such as laser-induced breakdown spectroscopy (LIBS) and laser-induced fluorescence (LIF) have also been used to obtain a complementary elemental and molecular composition in a non- or micro-invasive way for glass-based materials [17–25]. With some works focused on the parameters optimization for the analysis of model soda-lime silicate [19] and historical lead silicate glasses [24]. Other works focused more on the characterisation of chromophores and opacifiers of ancient glasses, and others on the degradation layers and processes [18, 20, 21]. LIBS is a micro-invasive technique that allows qualitative, semi-quantitative and quantitative material composition analysis. The analyse is done by the spectral analysis of the luminous plume generated by pulsed laser ablation of a small amount of material from the sample surface. [17, 26–28] Complemented with LIF in an entirely non-invasive approach, analytical information on trace elements and/or chromophores in glassy materials can also be obtained [17, 29–32].

Femtosecond laser-based techniques, such as non-linear optical microscopy (NLOM), in its various modalities of multiphoton excitation fluorescence (MPEF) and second and third harmonic generation (SHG and THG), are also a new set of non-invasive imaging techniques applied in the analysis of cultural heritage objects. [33–37] Due to their high peak power and short duration, these lasers favour non-linear optical processes without undesirable side effects, such as photobleaching and/or photo-toxicity damage [33]. With NLOM techniques, it is possible to obtain 3D compositional and structural information of a material based on the detection of fluorophores (MPEF) [33] of crystalline or highly organised structures without inversion symmetry (by SHG) [38]. The position of the boundaries of layers by virtue of the local differences in the refractive index and third-order non-linear susceptibility and dispersion (by THG) can also be obtained. [15, 39] NLOM is still insufficiently tested on glass objects despite these advantages. Only a known study explored the potential of combining all the above laser techniques (LIBS, LIF and NLOM-MPEF) for analysing glass pieces painted with grisailles [40]. In that study, the capability for non-invasive thickness measurement of different grisaille paint layers by NLOM with the MPEF modality was proven, as well as the determination of the elemental and molecular composition of the support glasses and their corresponding grisaille paints in a non- or micro-invasive way [40].

The main objective of this research was to characterise in a non-invasive way a set of selected stained-glass window samples with grisaille paints. The results of this characterisation, together with the compositions found in the literature, will help to achieve a better understanding of the evolution of the structure and composition of the grisaille paint throughout the centuries. This will directly correlate with the evolution of the technological production of this type of paint. At the same time, this study also intends to test and disseminate a new, rarely used, and innovative multi-analytical approach for the study of these cultural heritage materials.

Materials and methods

Samples

The twenty-three stained-glass window samples with grisaille paint selected to be analysed are shown in Fig. 1. The samples came from eight different collections: Joost Caen's private collection (JC) with samples from Low Countries (JC015a, JC020 and JC010), France (JC012) and Belgium (JC003 and JC007); Restoration atelier of Canterbury (LS)

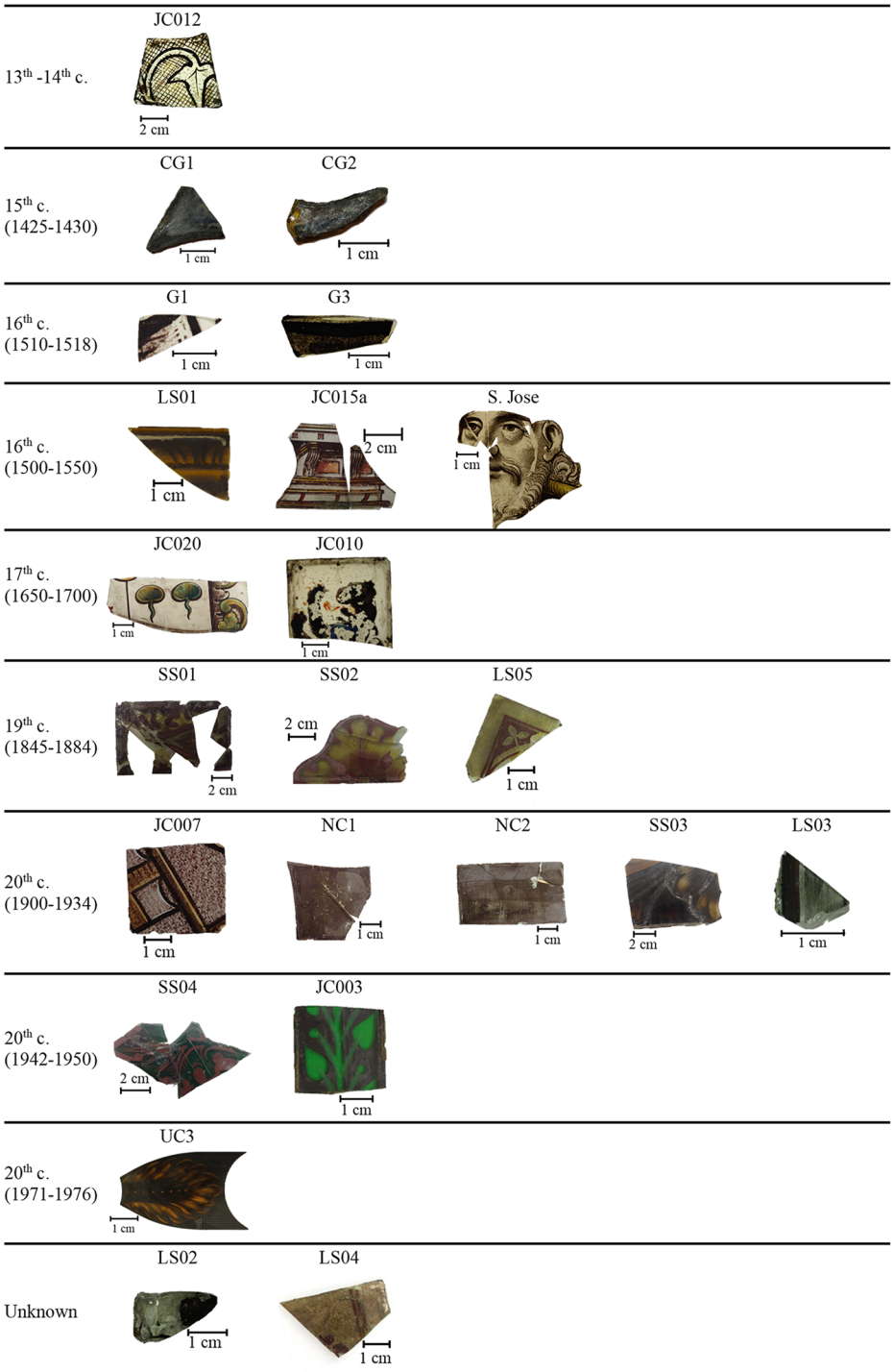

Fig. 1 Samples of grisaille paints on stained-glass windows studied in this work

with samples from France (LS01) and United Kingdom (LS02, LS03, LS04 and LS05); Glasmalerei Otto Peters atelier (SS) with samples from United Kingdom (SS01, SS02 and SS04) and Germany (SS03); Nidaros Cathedral (NC1, NC2) in Norway; Uppsala Cathedral (UC3) in Sweden; Church of Grodziec (CG1, CG2), in Poland; Convent of Tomar (G1, G3) in Portugal; and Batalha Monastery (S. José), also from Portugal. This group of samples allows a broad overview of the grisailles throughout Europe, with samples from nine countries covering chronologies from the 13th to the twentieth centuries, enabling the study of the evolution of this paint throughout time and place.

Analytical techniques

The stained-glass window samples and their corresponding grisaille paint layers were characterised by micro particle induced X-ray emission (μ-PIXE), micro energy dispersive X-ray fluorescence (μ-EDXRF), laser-induced breakdown spectroscopy (LIBS), laser-induced fluorescence (LIF), nonlinear optical microscopy in the modality of multiphoton excitation fluorescence (NLOM-MPEF) and optical microscopy (OM). With this multi-analytical and complementary approach, a comparison between the results obtained by these different techniques has allowed for a more complete and in-depth knowledge of the studied materials.

The glass supports and grisaille layers were analysed on their surface. Some selected samples were mounted in resin to be observed in cross-sections by optical microscopy. Data limitations were considered for the interpretation of the results, mainly for the lighter elements on the glass support and grisaille paint layers.

μ-EDXRF

To obtain the chemical composition of the samples support glasses, μ-EDXRF analyses were carried out. An ArtTAX, Intax®spectrometer (Brunker Nano GmbH, Berlin, Germany), equipped with an aircooled low-power X-ray tube with a Mo target and Xflash®Peltier (Brunker Nano GmbH, Berlin, Germany), cooled silicon drift detector, was used. The primary X-ray beam is focused to a diameter of 70 μm by means of a polycapillary X-ray mini lens. The spectrometer was operated at 40 kV, 0.6 mA, under a He flow atmosphere to optimise the detection of light elements with an acquisition time of 360 s. At least three different measurements were carried out on each different material. Depending on the element and on the matrix under analysis, the typical probing of the equipment can go from a few micrometers' (ca. 30 μm, e.g., lead-based glass) to some millimeters' depth (ca. 2–3 mm, e.g., borosilicate). Semi-quantitative analyses were carried out with the AXIL program, using spectra obtained from Corning Museum of Glass A, B, and D glass standards. The analytical capability of the equipment is limited to elements with atomic number $Z > 13$, thus making impossible the detection of boron, sodium, and magnesium. There is also lower accuracy in quantifying lighter elements, such as phosphorus. The concentration of sodium and magnesium was calculated by the method of 'matrix by difference' [41]. Some support glasses were previously analysed by Louro 2017 [42] (JC012, JC015a, JC020, JC007, SS04, JC003) and Delgado 2010 [43] (G1, G3, S.José), and their results were used to be compared with the rest of the samples.

μ-PIXE

The chemical composition of the grisaille paint layers was also assessed using μ-PIXE. They were made at the ion beam analytical facilities at the Instituto Superior Técnico (IST), Polo de Loures (Lisbon). A 2.5 MV Van de Graaff accelerator and an OM150 Oxford Microbeams Ltd. (United Kingdom), scanning nuclear microprobe was used mainly in the external beam configuration. Samples were irradiated with a 2 MeV proton beam focused down to 60×70 μm^2 and X-ray spectra were collected with an SDD detector. The microprobe beam scanning system allowed to obtain the elemental distribution maps in an area of 1×1 mm^2, and specific regions of interest were selected for quantitative analysis. The conditions used only permitted the quantification of elements with atomic number $Z > 11$. Operation and basic data manipulation were achieved using OMDAQ software; quantitative analysis was done with the GUPIX program. Each sample was analysed in three different zones, and the results in oxides weight percentage were normalised to 100 wt. %. In order to validate the obtained concentration results, the Corning C standard reference glass was also analysed.

LIBS

LIBS analyses were carried out both on the grisaille paint layers and glass support. They were conducted at IQFR-CSIC using laser excitation at 266 nm (4th harmonic of a Q-switched Nd:YAG laser (Lotis TII, LS-2147, Minsk, Belarus), 15 ns pulses, 10 Hz repetition rate). LIBS spectra were recorded using a 0.2 m Czerny-Turner spectrograph (Andor Technology, Belfast, Ireland, Shamrock Kymera-193i-A) equipped with a grating of 1200 grooves/mm (blazed at 500 nm) and coupled to a time-gated intensified charge-coupled device (ICCD) camera (Andor Technology, Belfast, Ireland, iStar CCD 334, 10241024 active pixels, 13 μm × 13 μm pixel). The ICCD detector is synchronised with the Q-Switch output electrical signal that triggers the laser pulse. The laser beam was directed to the surface of the samples by the use of mirrors at an incidence angle of 45°. Focusing with a 10 cm focal length lens allowed fluences as high as 9 J/cm^2 to be achieved. The shot-to-shot laser energy fluctuation was less than 10%. LIBS spectra were recorded at 50 nm intervals at single acquisition mode in the

230–300 nm, and step and glow mode in the 300–600 nm wavelength ranges. Spectra were recorded at a 0.2 nm resolution with a gate delay and width of 800 ns and 3 µs, respectively. For higher wavelengths ($\lambda \geq 300$ nm) a cut-off filter at 300 nm was placed in front of the entrance window of the spectrograph to reduce the scattered laser light from the surface of the sample and to avoid second-order diffraction. Spectra resulted from summing up the emissions of the products of ablation after ten successive laser pulses, a number that provided good signal/noise ratios.

LIF

LIF measurements were carried out using laser excitation at 266 nm (same laser source used for LIBS) and a 0.30 m spectrograph with a 300 grooves/mm grating (TMc300 Bentham Instruments Ltd., United Kingdom) coupled to an intensified charged coupled detector (2151 Andor Technologies, Belfast, Irland). The temporal gate was operated at zero-time delay with respect to the arrival of the laser pulse to the surface of the sample and with a width of 3 µs. The sample was again illuminated at an incidence angle of 45° with pulses of around 0.1 mJ using a 1×2 mm laser spot size. LIF spectra were recorded at 300 nm intervals in the wavelength range of 300–700 nm. Cut-off filters at 300 and 360 nm were used to reduce the scattered laser light from the surface of the sample and to avoid the second-order diffraction. Each spectrum resulted from the accumulation of 50 signals acquired at different points in each sample zone.

NLOM-MPEF

For NLOM-MPEF, a home-made non-linear optical microscope at IQFR-CSIC uses a mode-locked Ti: Sapphire femtosecond laser (Spectra physics lasers, California, USA) emitting at 800 nm, with average power of 680 mW, delivering 70 fs pulses at a repetition rate of 80 MHz as the excitation light source. A variable neutral density filter (NDC-50C-2 M, Thorlabs) serves to control the laser power reaching the sample. For the present measurements, the average power was in the range of 7–15 mW, values far from the damage threshold of the paint grisaille layers (as monitored through CCD online visualisation of the sample surface during the femtosecond laser excitation). The laser beam was modulated using a chopper at a frequency of 130 Hz and conducted to the sample through the aperture of a microscope objective lens (M Plan Apo HL $50\times$, Mitutoyo, NA 0.42) by using a dichroic beam splitter (FF750-SDi02-25×36, Semrock) with high reflection at 800 nm. The laser focal plane was selected with motorised translation XYZ stages (Standa 8MVT100–25–1 for XY and Standa 8MTF for Z, Standa, Lithuania). The lateral and in-depth resolutions achieved are of 1 and 2 µm, respectively. A LabVIEW interface was used to control both scanning and data acquisition procedures. The MPEF signals were collected in the backward direction through the microscope objective lens and a beam splitter (70/30) and measured using a photomultiplier tube (9783B, ET Enterprises, Japan) connected to a lock-in amplifier (SR810 DSP, Stanford Research Systems, USA) to ensure high amplification and good signal-to-noise ratio. A short band pass filter (335–610 nm, Thorlabs FGB37S) was placed at the entrance of the photomultiplier to cut-off the reflected laser light. The remaining 30% of the MPEF signal was sent to a CCD camera (Thorlabs DCC1645C) for online visualisation of the sample surface and the signal collection process. The thickness measurements were carried out in five different points of each sample in depth-scans (Z-direction) of the MPEF signal. For the samples G3, LS02 and LS04 no reliable measurements were able to be taken, probably due to irregularities on the painted surface.

OM

The preparation of the samples and the OM analysis was done in the facilities of the Polytechnic University of Catalonia—BarcelonaTech. A Nikon Eclipse LV100D (Japan) microscope equipped with a camera Infinity 1.3C was used. The polished sections were examined in reflected (bright and dark field) light. Only fragments where sampling was possible were mounted in resin and analysed by this technique: SS01, SS02, SS03, NC1, NC2 and UC3.

Results

Compositional characterisation

Support glasses

Even though this work mainly focuses on the characterisation of the grisaille paint layers, the chemical composition of the support glasses was also assessed for better comprehension of each sample and to better compare the grisailles painted on the different support glasses.

The distribution of the compositional types of the support glasses throughout the different chronologies is represented in Fig. 2. This classification was based on the results presented in the Supplementary material, Additional file 1: Table S1, and the diagrams of Schalm et al. [44], Dungworth [45], and Rodrigues [46] were considered to distinguish the presented classifications.

The compositions of the support glasses and their classification into the different types agree with what was expected for the chronology and provenance of each sample. The potassium-rich silicate glasses have the oldest chronologies (13–16th c.) and the soda-rich and soda-lime silicate glasses in the Modern samples (19–20th c.). An exception is the 16th-century samples from Portugal, either from the Convent of Tomar (G1, G3) and the Batalha Monastery (S.José), despite having an older chronology, are soda-rich glasses, which agrees with previous studies on glass samples from these stained-glass windows

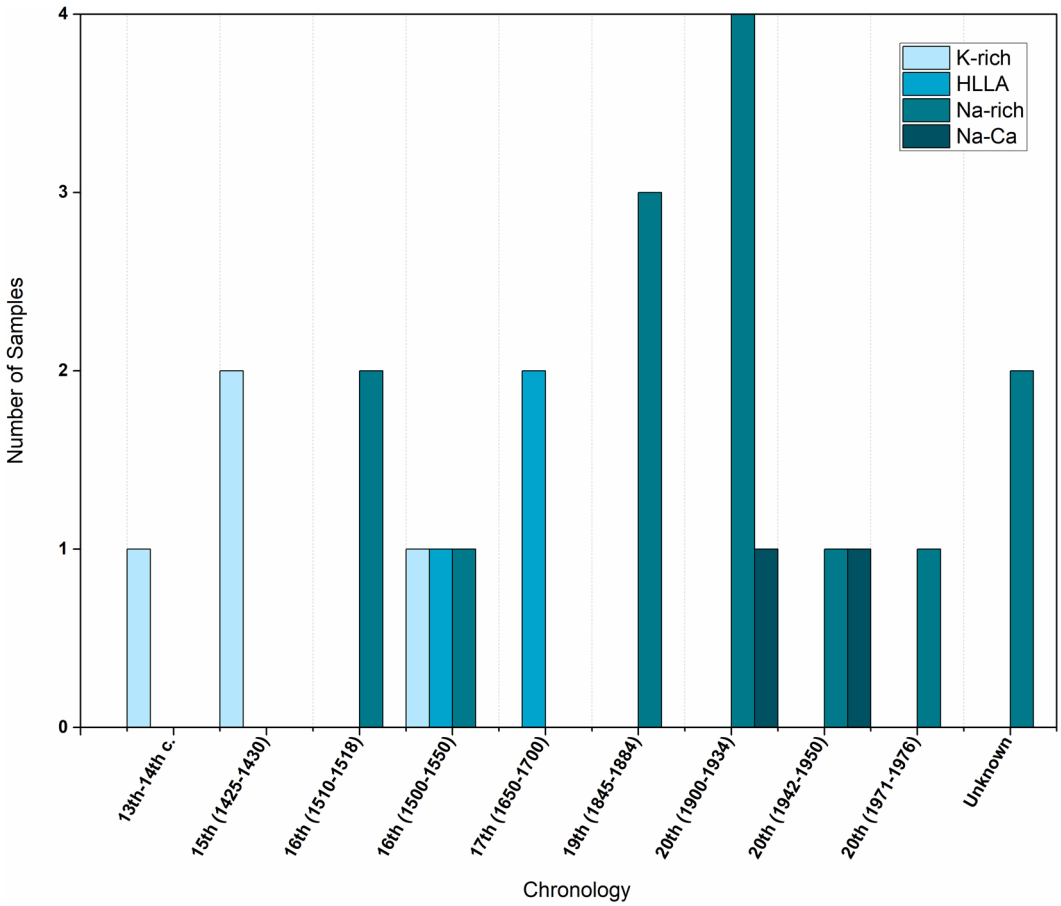

Fig. 2 Compositional types of glasses throughout different sample's chronologies. (K-rich = potash-rich silicate glass, HLLA = high-lime low-alkali glass, Na-rich = soda-rich silicate glass, Na-Ca = soda-lime silicate glass)

[47]. Three glasses dated from the sixteenth and seventeenth centuries (JC015a, JC020, and JC010) with high calcium content and relatively low sodium and potassium levels (Fig. 2 and Additional file 1: Table S1) were also identified. This high calcium content is usually present in high-lime low-alkali compositions. These samples come from the Low Countries and agree with the glass composition used during this period in this European region [44, 48].

The summary of the main elemental components of the support glasses of the samples as obtained by LIBS is presented in Table 1. These results were obtained by the assignment of the spectral emission lines based on the NIST database [49].

The LIBS spectra reveal the elemental composition by virtue of the emission lines of the major and minor components. These components are iron (Fe), silicon (Si), calcium (Ca), aluminium (Al), titanium (Ti), potassium (K), strontium (Sr), barium (Ba), sodium (Na), magnesium (Mg) and manganese (Mn). Si, Ca, Al, K, and Na correspond to the main glass components. Other elements (Mg, Fe, Mn, Ti, Sr, Ba) can be attributed to stabilising agents and impurities from the glass raw materials. The LIBS results corroborate the classifications given for each glass, as shown in Fig. 2, according to the main elements marked in Table 1. It was also possible to identify elements not detected by EDXRF, such as boron (B). This element, in low quantity, can also be associated with raw materials impurities [50, 51]. Silver (Ag) was also detected in the SS01 and SS02 samples, suggesting the presence of a common stained glass window decoration called yellow silver stain. This technique is responsible for different hues between orange and yellow on stained glass windows obtained by silver nanoparticle aggregates [52, 53].

Grisaille paint layers

Table 2 and Fig. 3 show the elementary composition of the grisaille paint layers and the normalised distributions of the different main components of the grisaille samples, respectively. These distributions were based on the composition's main elements and according to the different grisaille's components, the base glass (SiO_2, PbO) and the colouring agents

Table 1 Elemental composition of the support glasses of the samples determined by LIBS

Date	Name	Colour	Elemental composition
13th -14th	JC012	Colourless	**Si**, Fe, Mn, **Mg**, Ca, Al, Ba, Cu, Sr, Ti, B, **K**, Na, CaO
15th (1425–1430)	CG1	Blue	**Si**, Fe, Mn, Mg, Ca, Al, Ba, Cu, Sr, B, **K**, **Co**, Na, CaO
	CG2	Yellow	**Si**, **Fe, Mn, Mg,** Ca, Al, Ba, Sr, B, **K**, Co, Na, CaO
16th (1510–1518)	G1	Colourless	**Si**, Fe, Mn, **Mg, Ca**, Al, Pb, Ba, Cu, Sr, Ti, K, Na, CaO
	G3	Colourless	**Si,** Fe, **Mn**, Mg, **Ca**, Al, Ba, Sr, Ti, K, Na, CaO
16th (1500–1550)	LS01	Yellow	**Si**, Fe, **Mn, Mg, Ca**, Al, Ba, Cu, Sr, Ti, B, K, Zn, Na**,** CaO
	JC015a	Colourless	**Si**, Fe, Mn, **Mg, Ca, Al,** Ba, Cu, Sr, **Ti**, B, K, Ni, **Na**, CaO
	S.José	Colourless	**Si**, Fe, Mn, **Mg**, **Ca, Al**, Ba, Sr, Ti, K, Zn, Co, Na, **CaO**
17th (1650–1700)	JC020	Colourless	**Si**, Fe, Mn, **Mg**, Ca, **Al,** Ba, **Cu,** Sr, Ti, K, **Na**, **CaO**
	JC010	Colourless	**Si**, Fe, Mn, **Mg**, Ca, Al, Ba, Sr, Ti, K, Na, **CaO**
19th (1845–1884)	SS01	Colourless	**Si**, Fe, **Mn**, Mg, **Ca, Al**, Pb, Ba, Cu, **Ag**, Sr, Ti, B, **Zn,** Cr, **Na**, CaO
	SS02	Colourless	**Si**, Fe, Mn, Mg, Ca, Al, Ba, **Ag,** Sr, Ti, K, **Zn, Na**, CaO
	LS05	Yellowish	**Si, Fe, Mn,** Mg, **Ca**, Al, Ba, Sr, Ti, K, Cr, **Na**, **CaO**
20th (1900–1934)	JC007	Colourless	**Si**, Fe, Mg, **Ca,** Al, Sr, Sn, **Na**, CaO
	NC1	Greyish	**Si**, Fe, Mn, Mg, **Ca**, Al, Ba, **Cu,** Sr, Ti, K, **Na**, CaO
	NC2	Greyish	**Si**, Fe, Mn, Mg, **Ca**, Al, Pb, Ba, **Cu,** Sr, Ti, K, **Na**, CaO
	SS03	Colourless	**Si**, Fe, Mn, Mg, **Ca**, Al, Pb, Ba, **Cu,** Sr, Ti, K, **Cr**, **Na**, CaO
	LS03	Colourless	**Si**, Fe, Mn, Mg, **Ca**, Al, Pb, Ba, Cu, Sr, Ti, K, **Na**, CaO
20th (1942–1950)	SS04	Green	**Si**, Fe, Mn, Mg, **Ca**, Al, Sr, **Na**, CaO
	JC003	Green	**Si**, Fe, Mn, Mg, Ca, Ba, **Cu,** Sr, **Ti**, K, **Zn**, Cr, **Na**, **CaO**
20th (1971–1976)	UC3	Yellow	**Si**, Fe, Mn, **Mg, Ca**, Al, Ba, Sr, Ti, **Na**, **CaO**
Unknown	LS02	Colourless	**Si**, Fe, Mn, Mg, **Ca**, Al, Pb, Ba, Cu, Sr, Ti, B, K, **Na**, CaO
	LS04	Colourless	**Si,** Fe, **Mn**, Mg, **Ca**, Al, Ba, Sr, **Ti,** K, **Na**, **CaO**

The main components are indicated inbold

(Fe_2O_3, CuO, CoO, Cr_2O_3, MnO). The ZnO content was considered either for the base glass or colouring agents.

With the grisailles composition (Table 2), it was possible to see that all grisailles were mainly constituted by a mixture of a high-lead silica base glass, with a mixture of metal oxides (Fe_2O_3, CuO, CoO, Cr_2O_3, MnO) which are responsible for the grisaille's colouration. The rest of identified oxides (Table 2) could be associated with compounds introduced to the grisailles formulations as stabilisers agents for the base glass, raw materials impurities or/and elements from compounds that lixiviated from the support glass to the grisaille matrix [8, 9, 40, 52]. The identification of AgO in the CG1, CG2, JC010, and UC3 grisailles can indicate the presence of yellow silver stain, in the glass under the grisaille layer. Some grisailles also present a high quantity of SO_3 (SS02 and SS04), which can indicate the presence of crystal deposits on the surface of the grisaille paint. These deposits are usually formed through the support or base glass network breakdown. The alkali or earth-alkali leached ions on the surface will interact with SO_2 from the environment and form crystals on top of the grisaille layer [6, 54, 55].

JC010 grisaille also presents an overall composition distinct from the other samples (Table 2), with a higher SiO_2 and K_2O concentration and a lower PbO concentration, as well as the identification of a significant As_2O_5 value and the presence of Bi_2O_3. All these characteristics make it closer to an enamel composition than a grisaille one. Being this possibility discussed further.

From the overall grisailles composition (Table 2), it was also possible to see that concentrations between ~ 40 wt. % and 82 wt. % comprehend the main base glass components (SiO_2 and PbO), which agree with well-balanced grisailles [56]. The proportion between the different components of the grisaille (base glass and colouring agents) is of great importance for the paint stability. The quantity of base glass must be enough to cover all the metal oxide grains and to guarantee good adhesion of the grisaille to the substrate [56].

As described before, the base glasses of the grisaille's formulation were mainly constituted by SiO_2 and PbO. Most of the base glasses present concentrations between 40 and 60 wt. % of SiO_2 to PbO, as seen in Fig. 3a. This agrees with the range of proportions previously identified in the base glasses of historical grisaille samples [3]. However, it disagrees with the historical written sources, which usually describe the production of the grisaille base glass with higher quantities of lead oxide (3:1 PbO to SiO_2) [1]. This difference could have various explanations: the lead volatilisation during the firing

Table 2 Composition (wt. %) of the grisailles analysed by PIXE

Date	Name	Al_2O_3	SiO_2	P_2O_5	SO_3	Cl	K_2O	CaO	TiO_2	Cr_2O_3	MnO	Fe_2O_3	CoO	NiO	CuO	ZnO	As_2O_5	ZrO_2	AgO	SnO_2	BaO	PbO	Bi_2O_3
13th–14th	**JC012**		27.0		9.55	1.20	1.08	2.41	0.08	0.01	0.08	29.0		0.03	0.43	0.09						31.5	
15th (1425–1430)	**CG1**	7.34	23.3	5.28	1.28	1.11	1.53	15.2	0.20		0.21	5.37	0.03	0.03	20.0	0.08			0.36	0.42	0.21	17.8	
	CG2	4.78	29.8	1.79	1.37	0.59	6.70	18.8	0.22		0.39	2.98	0.03	0.03	14.1	0.11	0.27		0.60	1.22	0.13	16.6	
16th (1510–1518)	**G1**		25.6		2.20	2.28	1.29	4.17	0.10		0.15	28.6			6.25	0.94				0.60		28.7	
	G3		28.6	2.50	5.20	1.64	2.24	9.86	0.12		0.38	24.4			4.26	0.73					0.09	20.4	
16th (1500–1550)	**LS01**		23.1			1.03	1.66	4.79	0.22		0.10		1.10		3.55	0.99						31.4	
	JC015a		23.9	2.50	3.90	0.65	0.96	2.73	0.10	0.01	0.14	38.9		0.04	4.21	2.17					0.07	23.6	
	S. José		13.8		12.5	2.46	1.29	6.77	0.09	0.33	0.66	32.8			4.19	1.64					0.02	27.1	
17th (1650–1700)	**JC020**		19.6	2.67	7.65	1.41	1.95	8.56	0.19		0.31	26.9			2.63	1.16					0.05	28.6	
	JC010		59.0		2.50	0.75	11.5	4.42	0.10		0.10	5.45	4.97	1.20	2.06	0.08	3.19		1.07		0.03	3.37	1.47
19th (1845–1884)	**SS01**		42.0		4.00	2.34	1.61	1.53	0.05		0.36	16.1	0.67	0.03	0.04	0.04					0.04	33.3	
	SS02		13.5		19.7	0.68	0.13	0.64	0.03		0.02	21.6		0.01	0.02	0.06					0.02	43.5	
	LS05		38.5		10.8	0.40	0.87	1.70	0.08	0.02	1.30	15.9	0.35	0.02	0.04	0.16					0.05	29.8	
20th (1900–1934)	**JC007**		25.7		7.63	0.78	1.27	8.62	0.09	0.02	4.91	17.5			2.04	0.50					0.32	29.7	
	NC1		20.1			0.38	0.12	0.62		3.68	0.02	9.81	8.33	0.38	0.22	0.13						55.6	
	NC2		72.8				0.96	7.25	0.04	0.63	0.02	3.41	3.34	0.16	0.3	0.03	0.21				0.06	9.32	
	SS03		55.3		1.83	0.30	0.27	2.95	0.11	2.09	0.36	14.7	0.51	0.01	0.02	2.44				1.28	0.02	17.9	
	LS03		41.4		3.05	0.60	0.81	7.05	0.12	0.11	1.83	10.6	4.59	0.19	1.66	0.07					0.13	27.7	
20th (1942–1950)	**SS04**		17.7		16.8	1.22	0.58	2.99	0.06	2.11	2.31	6.31	1.74	0.10	4.83	0.13					0.11	42.9	
	JC003		44.7		0.78	0.26	1.3	8.65	0.11	0.21	4.36	10.6			0.62	0.3	0.36				0.25	27.3	
20th (1971–1976)	**UC3**	3.99	28.0				0.16	0.47	0.18	5.07	0.39	8.71	5.28	0.15	0.03	5.32		0.30	1.15	1.71		38.9	
Unknown	**LS02**		23.7		8.83	0.89	0.30	7.56	0.07	0.03	4.25	11.1	2.31	0.12	0.08	0.92					0.18	39.5	
	LS04		28.3			11.02	2.22	1.56	0.08		1.89	20.2	0.26	0.02	0.04	0.26					0.07	34.0	
Cmog C			36.7		1.1	0.53	2.6	4.7	0.55			0.29	0.18	0.02	1.16	0.04					11.4	40.3	
[a]Error (%)			13		42	12	1.7	1.1	7.7			2.8	3.9	17	1.4	18					1	1	

[a] Fitting and counting statistics error (%)

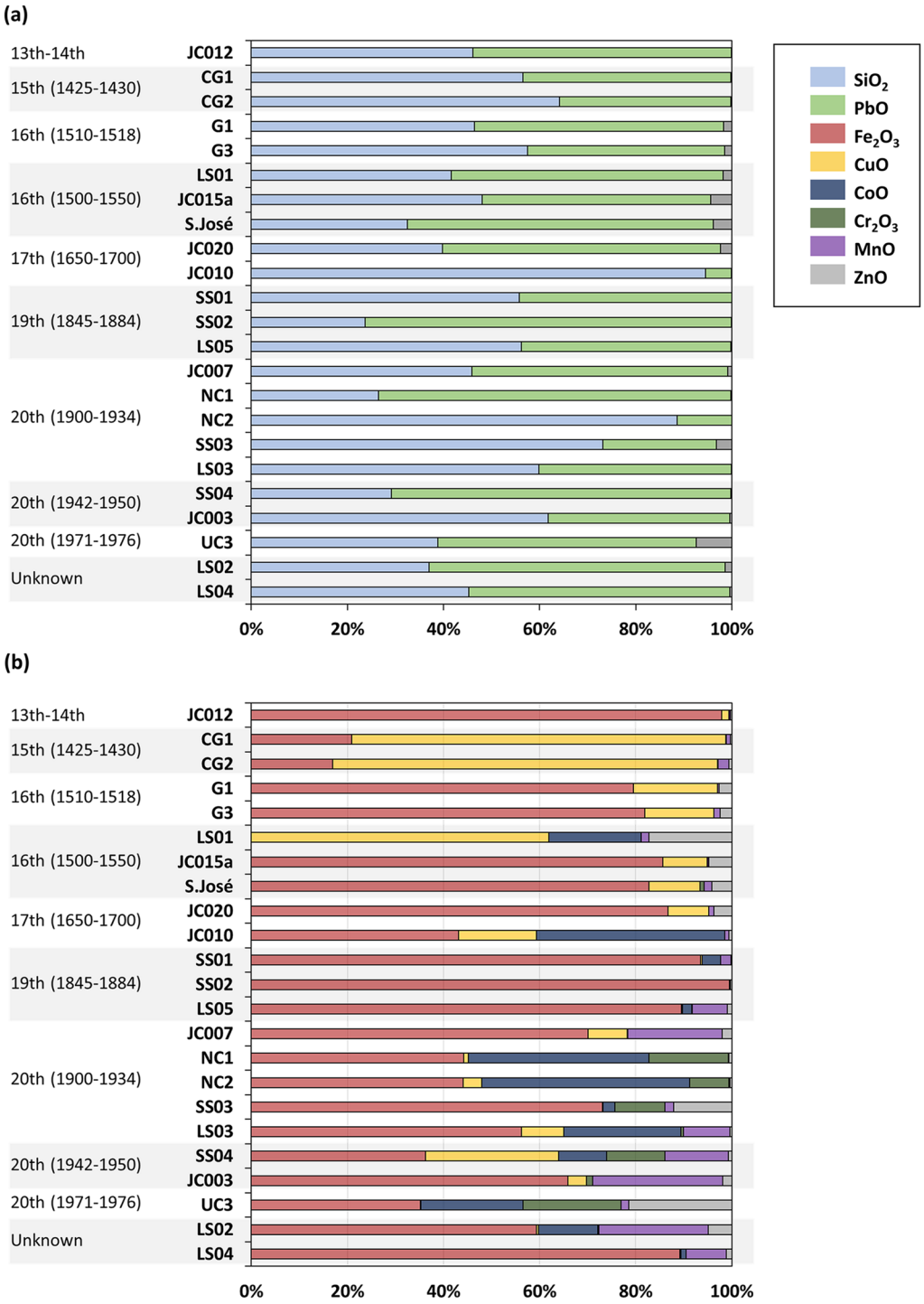

Fig. 3 Normalised distributions of different components of the grisailles: (**a**) base glass components, (**b**) metal oxides used as colouring agents

process; the result of a degradation process that leaves a silica-enriched base glass; or the introduction of different compounds, such as borax ($Na_2B_4O_7{\cdot}10H_2O$), to help to decrease the firing temperature, no longer needing for a base glass with higher amounts of lead. [13, 55–57] The samples JC010 and NC2 present more than 80 wt. % of silica in the base glass composition Fig. 3a. The grisaille layer thickness could influence this. When too thin, the support glass could interfere with the reading of the grisaille composition.

The normalised distribution of the various components that could be responsible for the colouration of the grisailles is shown in Fig. 3b. Iron oxide is the main component identified, followed by copper oxide Fig. 3b. This identification also agrees with what was previously reported in historical grisaille samples and with what is described throughout grisaille recipes across historical written sources [1, 3]. It was also possible to detect other compounds that could be used as colouring materials, such as cobalt, manganese, and chromium, mainly from samples from the seventeenth century onwards Fig. 3b. Contrary to iron and copper, cobalt and chromium were never described in the historical recipes, despite their use being previously identified in historical samples from the nineteenth and twentieth centuries [3, 8, 13, 58, 59]. Regarding manganese, it is possible to find mention of it being used in historical recipes from the 17th-century treatise *Ars Vitraria Experimentalis* by Johannes Kunckel [1, 60].

The zinc content was either considered as part of the base glass or as a colouring agent. Zinc could be introduced with the copper if a Cu–Zn alloy (brass) could be used instead of pure copper as the colouring agent or as an impurity from cobalt ores [6, 61, 62]. Zinc could also be introduced as a component of the base glass, as it can help the melting process, mainly associated with boron [63, 64].

The summary of the main elemental components of the grisaille paint layers, as obtained by LIBS is presented in Table 3. As previously explained for the support glasses, these results were obtained by assigning the spectral emission lines based on the NIST database [49].

The LIBS spectra allow the identification of the grisaille composition through the emission lines from their main components and possible impurities. The main elements identified throughout the samples were silicon (Si) and lead (Pb) (Table 3), being the main constituents of the grisailles base glass matrix, as previously mentioned. Iron (Fe) is also one of the main elements identified throughout the grisaille samples, usually, together with copper (Cu), manganese (Mn), cobalt (Co), and chromium (Cr) (Table 3). This confirms the PIXE analysis results regarding the oxides responsible for the colouration of these paint layers (Fig. 3 and Table 2). The rest of identified elements (Na, Mg, Al, K, Ca, Ti, Zn, Sr, Ba), could represent compounds introduced to the grisailles as stabilisers agents for the base glass, raw materials impurities or/and elements from compounds that lixiviated from the support glass to the grisaille matrix [8, 9, 40, 52].

It was also possible to identify the boron (B) in two samples, SS03 and UC3, as this was not detected by PIXE analysis due to its low X-ray energy. The identification of boron

Table 3 Elemental composition of the grisaille paint layers as determined by LIBS

Date	Name	Elemental composition
13–14th	JC012	**Si**, **Fe**, Mn, Mg, Ca, **Al**, **Pb**, Ba, **Cu**, Ag, Sr, Ti, K, Ni, Na, **CaO**
15th (1425–1430)	CG1	**Si, Fe**, **Mn**, **Mg**, Ca, Al, **Pb**, Ba, **Cu**, Sr, **Ti**, K, Na, CaO
	CG2	**Si, Fe**, **Mn**, Mg, **Ca**, Al, **Pb,** Ba, Cu, Sr, Ti, K, Na, CN, C_2, CaO
16th (1510–1518)	G1	**Si, Fe**, **Mn**, Mg, **Ca,** Al, **Pb,** Ba, **Cu,** Sr, Ti, K, **Zn**, Cr, Na, CaO
	G3	**Si, Fe**, **Mn**, Mg, **Ca,** Al, **Pb**, Ba, **Cu,** Sr, Ti, K, Zn, Co, Cr, Na, CaO
16th (1500–1550)	LS01	**Si, Fe**, Mn, Mg, **Ca, Al, Pb,** Ba, **Cu,** Sr, Ti, K, Cr, Na, CaO
	JC015a	**Si, Fe**, Mn, Mg, Ca, Al, **Pb**, Ba, **Cu**, Sr, Ti, K, Cr, Na, CaO
	S.José	**Si, Fe**, Mn, **Mg,** Ca, Al, **Pb**, Ba, Cu, Sr, Ti, K, Zn, Co, Cr, **Sn, Na**, **CaO**
17th (1650–1700)	JC020	**Si**, **Fe**, Mn, Mg, Ca, Al, **Pb**, Ba, **Cu**, Sr, Ti, K, Cr, Na, **CaO**
	JC010	**Si, Fe**, Mn, Mg, Ca, Al, **Pb**, Ba, **Cu,** Sr, **Ti**, K, Ni, **Na,** CaO
19th (1845–1884)	SS01	**Si**, **Fe, Mn**, Mg, Ca, Al, **Pb**, **Ba**, Cu, Ag, Sr, Ti, K, **Co**, Cr, **Na**, CaO
	SS02	**Si**, **Fe**, Mn, Mg, Ca, Al, **Pb**, **Ba**, Cu, Sr, K, Ni, Cr, Na, CaO
	LS05	**Si**, **Fe**, **Mn**, Mg, Ca, Al, **Pb,** Ba, Cu, Sr, Ti, K, **Co, Ni**, Cr, CaO
20th (1900–1934)	JC007	**Si**, **Fe**, Mn, Mg, Ca, Al, **Pb**, **Ba**, Cu, Sr, Ti, K, Cr, Na, CaO
	NC1	**Si**, Fe, Mn, Mg, **Ca,** Al, **Pb,** Ba, **Cu,** Sr, Ti, K, **Co**, Na, **CaO**
	NC2	**Si**, Fe, Mn, Mg, **Ca**, Al, **Pb**, Ba, Cu, Sr, K, **Co,** Ni, **Cr**, Na, **CaO**
	SS03	**Si, Fe**, Mn, Mg, Ca, Al, **Pb,** Ba, Cu, Sr, Ti, B, K, **Co**, **Cr**, Sn, Na, CaO
	LS03	**Si**, Fe, **Mn**, Mg, Ca, Al, **Pb**, Ba, **Cu,** Sr, **Ti**, K, Zn, **Co, Cr**, **Na**, CaO
20th (1942–1950)	SS04	**Si**, Fe, Mn, Mg, Ca, Al, **Pb, Ba, Cu**, **Sr**, Ti, **K, Co, Cr**, Na, CaO
	JC003	**Si**, Fe, **Mn**, Mg, Al, Ca, **Pb,** Ba, **Cu,** Sr, K, **Zn, Co**, Cr, Na, CaO
20th (1971–1976)	UC3	**Si**, **Fe**, Mn, Mg, **Al**, Ca, **Pb,** Ba, Cu, **Ti**, B, **Co,** Ni, **Cr**, **Na**
Unknown	LS02	**Si**, **Fe, Mn,** Mg, Al, Ca, **Pb**, Ba, Cu, Sr, Ti, K, Zn, **Co**, **Na**, CaO
	LS04	**Si**, **Fe**, Mn, Mg, Al, Ca, **Pb**, Ba, Cu, Sr, Ti, K, Co, Cr, Na, **C_2**

The main components are indicated in bold

in these grisailles, which are also the ones with the highest amount of zinc oxide (Fig. 3 and Table 2), could indicate that an enamel made by lead–zinc borosilicate glass was used as base glass instead of a lead-silica glass [65].

LIF spectra of samples representing each chronology, including the support glass and the corresponding grisailles, are shown in Fig. 4. The spectra showed a broad feature between 300 and 700 nm, notwithstanding the specific characteristics of each sample related to its chemical composition.

Two broad emission bands between 300 and 500 nm were identified in the collected spectra and could be assigned to oxygen deficiency centres (ODC) from the glass network [30, 66, 67]. The band around 360 nm appearing both in

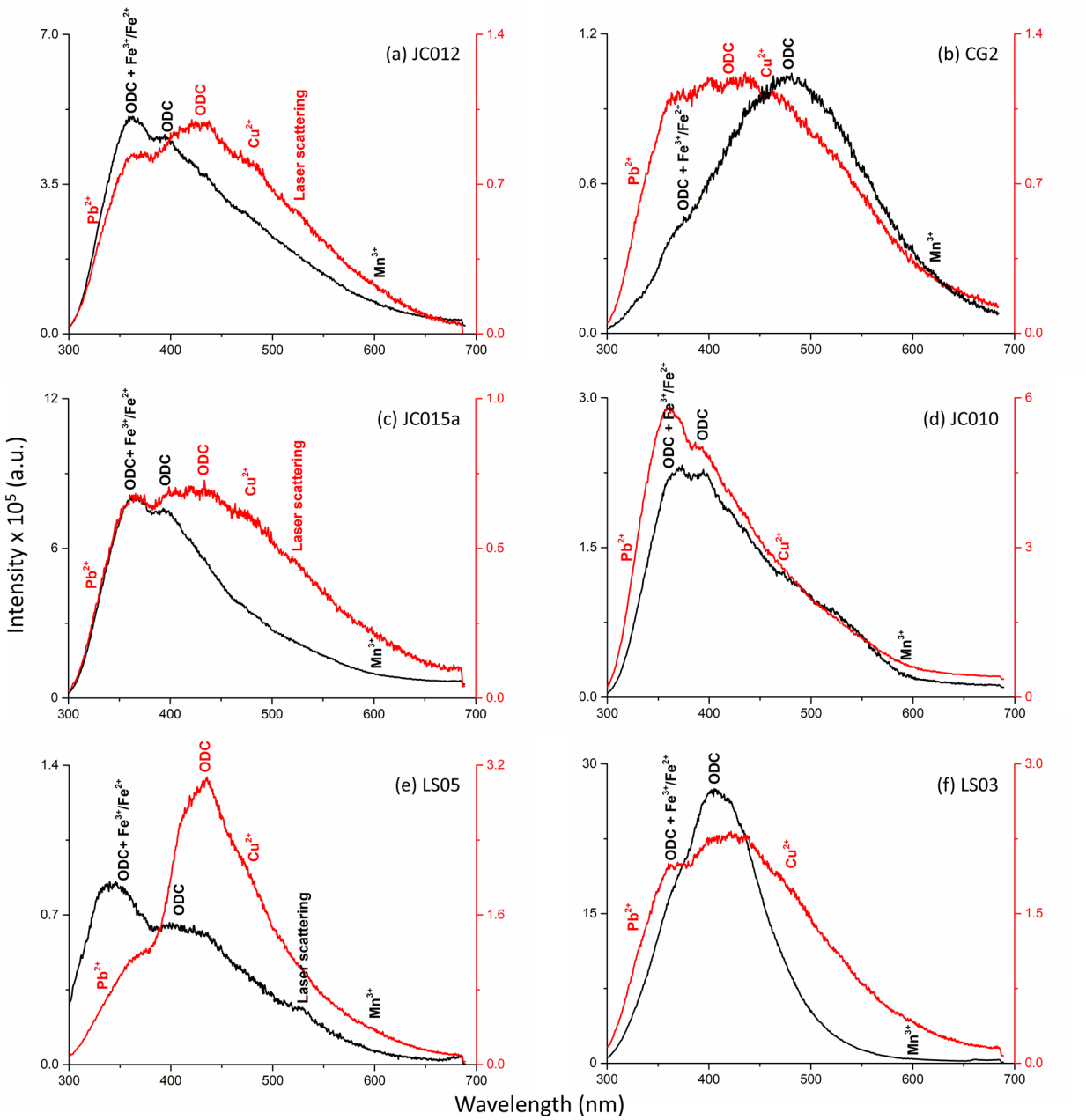

Fig. 4 LIF spectra from selected samples of glass support (in black) and the corresponding grisailles (in red). The bands refer as ODC indicates oxygen deficiency centres. The ions marked in red are only identified in the grisaille spectra, and the black ones can be identified in both grisaille and support glass. (**a**–**f**) correspond to LIF spectra of samples JC012, CG2, JC015a, JC010, LS05, LS03 representative of each chronology studied. Laser scattering: double wavelength of incident laser light

the glass and grisaille spectra, for all the samples, can also include a contribution from Fe^{2+}/Fe^{3+} chromophores [17].

The grisaille spectra on all the samples (red lines) present a wider and broader feature with an additional shoulder at around 330 nm, which could be assigned to the Pb^{2+}, revealing the main component of the grisailles composition, as proved by PIXE (Fig. 3 and Table 2) and LIBS (Table 3) analysis. [31, 68] The LIF spectra also include the contribution of a band around 475 nm that can be ascribed to the presence of Cu^{2+} chromophores, with a distinct presence in the grisailles composition [17].

Despite the presence of a higher variety of chromophores in the grisailles from the twentieth century, as those based on cobalt, chromium, and manganese (Fig. 3 and Table 3), the fluorescence emission from these could not be found in the LIF spectra (Fig. 4(f). This could be due to the reabsorption of the fluorescence emitted by these ions, as they all have absorption bands in the near-UV and Visible spectral ranges [69].

Morphology and thickness

Figure 5 shows the microscopic images of the cross-sections of the fragments taken from the sample and mounted in resin (SS01, SS02, NC1, NC2, SS03, UC3). In the images, it is possible to appreciate the rough surface of these samples and the high heterogeneity of the paint layers, with the presence of bubbles and various crystalline compounds that could correspond to the colouring agents. Comparing the

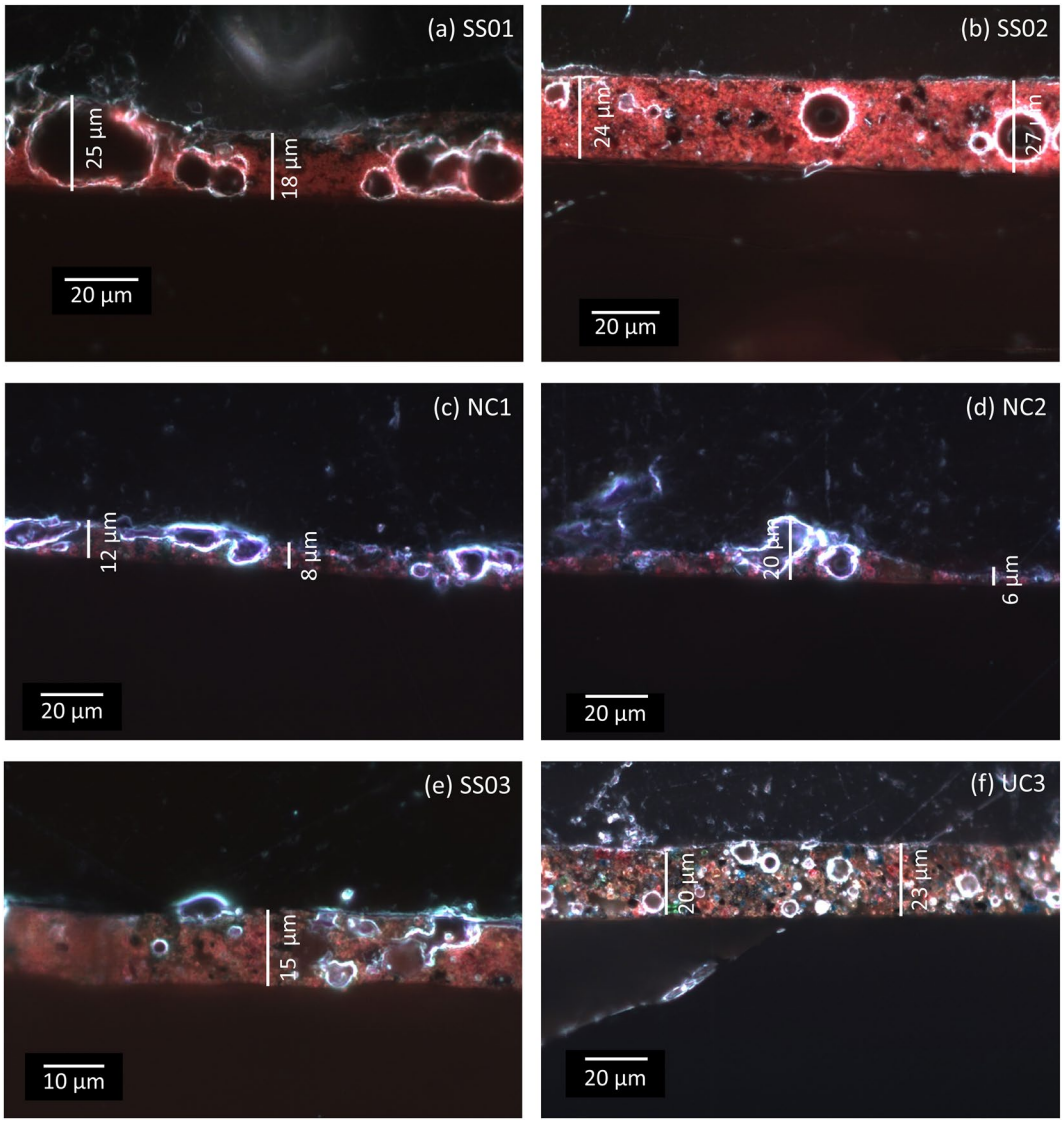

Fig. 5 OM cross-section images of the samples (**a**) SS01, (**b**) SS02, (**c**) NC1, (**d**) NC2, (**e**) SS03 and (**f**) UC3. These images were obtained by reflected light in dark field

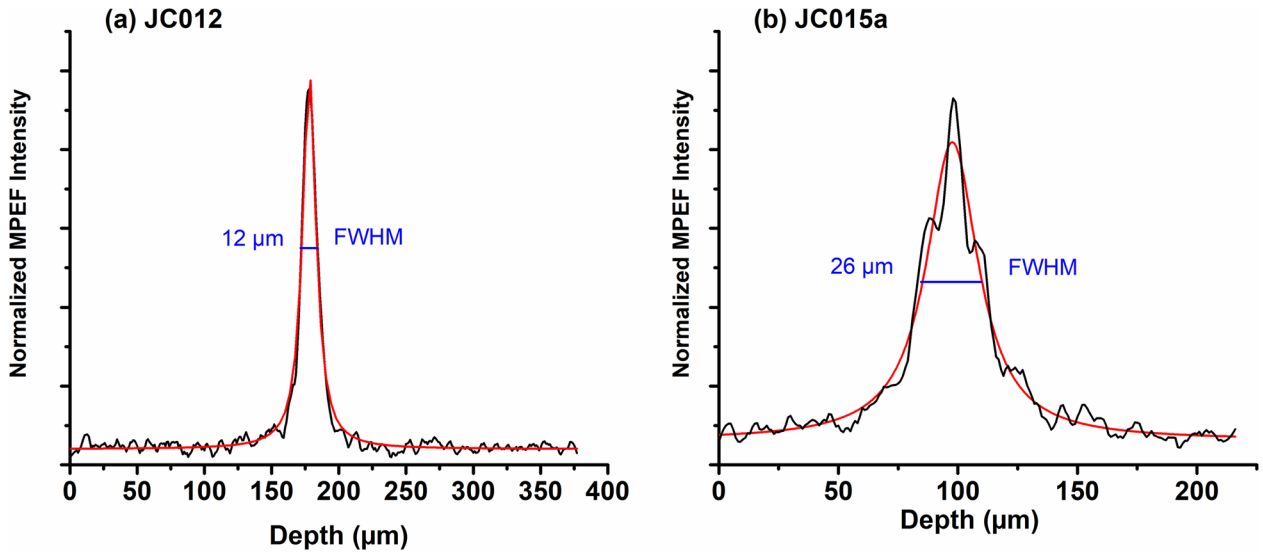

Fig. 6 Example of depth scans of the NLOM-MPEF signals (black line) on the grisaille paint layers from samples JC012 (**a**) and JC015a (**b**). The Lorentzian function fit is marked in red. The FWHM values of the fits after refractive index correction, which give the values of thickness, are indicated in blue

morphological appearance of these samples with the chemical results (Fig. 3 and Table 3), it is possible to understand that the grisailles, mainly constituted by iron Fig. 5(b), present a more homogeneous red layer. In contrast, grisailles, with a higher variety of colouring agents Fig. 5(f), present a heterogeneous layer with aggregates of different colours, red from iron, blue spots related to cobalt and green ones to chromium.

The cross-sections also allow the measurement of the grisailles layer thickness to be compared with the results obtained by the non-invasive technique NLOM-MPEF.

As revealed by the microscope images (Fig. 5), the grisailles are rather heterogeneous, and both their surface and thicknesses are uneven, so the MPEF in-depth scans were acquired in at least five different areas in each sample. Figure 6 shows examples of profiles taken from the samples JC012 and JC015a. The fitting using a Lorentzian function allowed the determination of the apparent paint layer thickness by means of the full width at half maximum (FWHM) [40]. The real thickness of the grisailles was calculated by correcting the FWHM value with the apparent depth correlation factor **F**, which considers the effective numerical aperture **NA** of the focusing objective lens and the refractive index **n** of the analysed material (Eq. 1). [70, 71]

$$F = \frac{1 - \sqrt{1 - NA^2}}{\mathrm{n} - \sqrt{n^2 - NA^2}} \quad (1)$$

The correlation factor **F** of grisaille paints was previously determined by Oujja et al [40] with a value of around 2. Table 4 shows the resulting thickness values obtained by MPEF for the samples analysed and their comparison with those obtained through optical microscopy images of the cross-sections.

The MPEF results, represented in Table 4, show the wide range of thicknesses that the grisaille paint layers could have, even throughout the same sample. This thickness variety can be explained by the heterogeneity of the paint layers themselves, as observed in the OM cross-section images (Fig. 5), and by the application of this paint on the glass (manually by a glass painter). The great range of values across the same sample is also the result of the two different ways in which the grisaille was used. In most cases, the grisailles used to create outlines (*grisaille á contourner*) doubles the thickness compared to the grisaille used for the shadows (*grisaille á modeler*).

The comparison of the thickness obtained by MPEF with those retrieved from OM, reveals a good agreement between the two sets of measurements. The OM results generally show a smaller range when compared with the MPEF results. This could be due to the limited sample fragment mounted in resin for OM measurements. At the same time, NLOM-MPEF can access all the sample surface, thus allowing for better representativity of the total range of thicknesses present in the same painted layer of the same sample.

Discussion

Grisaille paint layers composition and evolution

In the ternary graph, shown in Fig. 7, it is possible to see the distribution of the grisailles according to their composition,

Table 4 Ranges of thickness of grisaille paint layers measured by NLOM-MPEF (measurements taken from 5 spots along the grisaille surface) and comparisons (when possible) with the OM measurements

Date	Name	Thickness in µm	
		by MPEF	by OM
13–14th	JC012	9–12	–
15th (1425–1430)	CG1	14–28	–
	CG2	12–36	–
16th (1510–1518)	G1	32–52	–
16th (1500–1550)	LS01	34–60	–
	JC015a	16–27	–
	S. José	27–64	–
17th (1650–1700)	JC020	28–47	–
	JC010	24–52	–
19th (1845–1884)	SS01	14–36	18–25
	SS02	10–32	24–27
	LS05	20–50	–
20th (1900–1934)	JC007	38–52	–
	NC1	10–17	8–12
	NC2	7–12	6–20
	SS03	14–22	15
	LS03	18–52	–
20th (1942–1950)	SS04	17–50	–
	JC003	12–30	–
20th (1971–1976)	UC3	10–20	20–23

considering that the grisailles compositions obtained can present changes regarding their original composition due to the possible presence of degradation products. In general, the grisailles tend to group according to their chronology not only when they have the same provenance but also when their provenance differs. The 15th-century samples (CG1, CG2) are the ones that stand out more markedly. The key difference between these and the rest of the samples is the use of copper oxide as the main colourant. However, the preference for copper in these samples is not related to their chronology but to their provenance, as both came from the Church of Grodziec (Poland). Previous studies verified that in countries from central and south-central Europe (Germany, Poland, Italy, and Czech Republic), the use of copper as the main colourant of the grisaille was preferred [3, 10, 55, 72]. The sample from the 13–14th centuries (JC012), of French origin, also has a similar composition to that of grisailles from the same provenance and chronologies from the church of *Sainte Chapelle* in Paris (France), studied by Verità et al. [73].

The 16th-century samples are also grouped according to their more specific chronology from 1510 to 1518 (G1, G3) and 1500–1550 (JC015a, S. José). Only sample LS01 is further from the group (Fig. 7). The samples, in this case, have different provenances, as samples G1, G3 and S. José are from two different monuments in Portugal, the Convent of Tomar (G) and the Batalha Monastery (S. José), and sample JC015 is identified as coming from the Low Countries. Nevertheless, they have similar compositions (Fig. 7 and Table 2), high quantities of (~ Fe_2O_3 24–39 wt. %), and lower quantities of CuO (~6–4 wt. %). These compositions also agree with those found in the literature for grisailles from the same chronology and provenance [47, 74, 75]. It is known that Flanders (a region that in the sixteenth century encompassed all the regions of Low Countries, Belgium, and Luxembourg) [48] at that time was exporting not only their glass and stained glass but also their technical expertise throughout Europe, including to Portugal. This led to a transference of knowledge that can justify the similarity between the Portuguese and Low Countries grisailles, even if the support glasses have different compositions. [47, 48] LS01 is identified as being from the sixteenth century. However, its composition, without iron and with a high amount of cobalt, is more similar to 19th and 20th-century compositions (Fig. 3), suggesting the possibility of a misattribution of the date.

Contrary to what was previously observed, the 17th-century grisailles could not be grouped, as shown in Fig. 7, despite having the same chronology and provenance (Low Countries). The JC020 grisaille has a composition closer to what was observed for the Low Countries sample, JC015, from the sixteenth century, with similar proportions between the base glass and components of the colouring agents (Fig. 3). The JC010 paint layer sample presents not only a different composition from its 17th-century counterpart (JC020) but also when compared with all other analysed grisailles (Table 2). With higher amounts of SiO_2 (~ 59 wt. %), K_2O (~ 11 wt. %), As_2O_5 (~ 3 wt. %), and NiO (~ 1.2 wt. %) and a lower amount of PbO (~ 3 wt. %). This grisaille also presents similar concentrations of Fe_2O_3 and CoO (~ 5 wt. %), a low concentration of CuO (~ 2 wt. %), and Bi_2O_3 was also detected (~ 1.5 wt. %). The presence of arsenic, nickel, and bismuth oxides can be related to typical contaminants accompanying the CoO on the smalt or zaffre, proving that one of these two cobalt pigments was used in this paint production [76]. The higher amount of K_2O can be related to using potassium-rich compounds, such as wood ash or potassium tartar, to lower the melting temperature and compensate for the low lead concentration [76]. The described composition is more similar to an enamel composition than a grisaille paint layer, indicating that the JC010 paint layer was wrongly identified as a grisaille when it probably is a dark enamel [76, 77].

Regarding the samples from the nineteenth and twentieth centuries, they generally present fewer quantities of iron and copper oxides (Fig. 7) due to the new colouring agents, such as cobalt, chromium, and manganese (Fig. 3), as mentioned before. This change is visible towards these chronologies and transversal to the different provenances (United

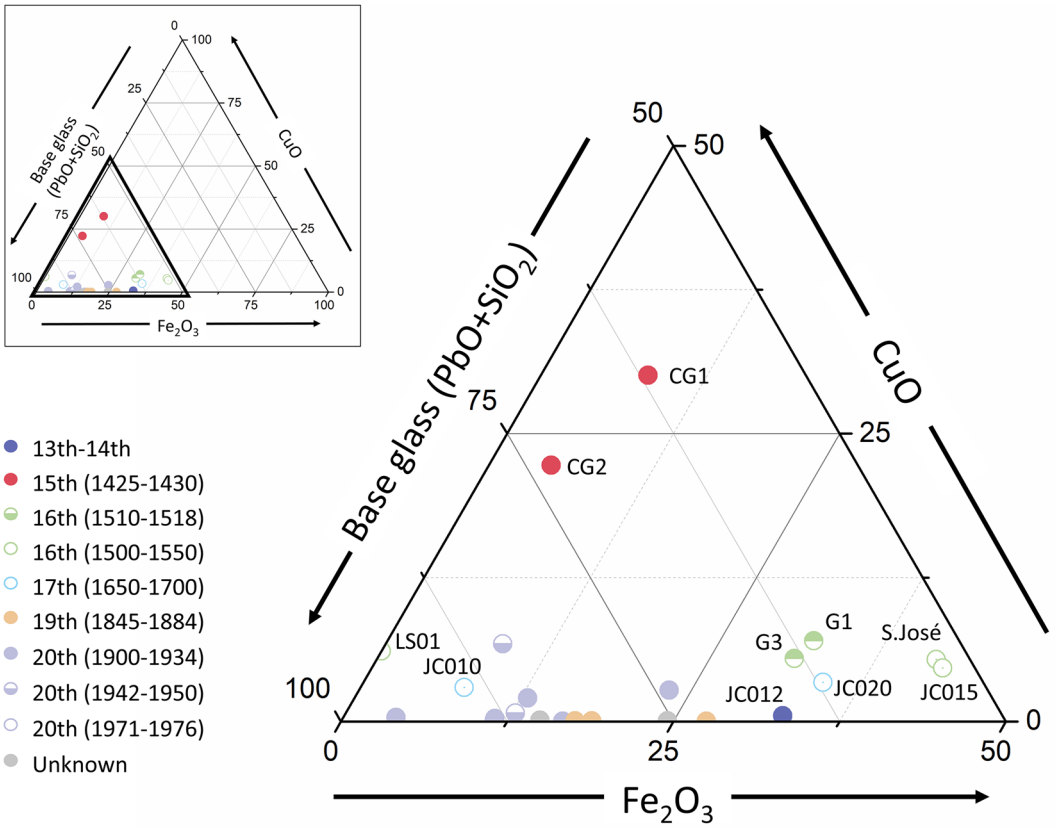

Fig. 7 Ternary plot of the main elements of the base glass ($PbO + SiO_2$) versus the iron and copper oxide showing the dispersion of the grisailles studied

Kingdom, Belgium, Norway, Germany, and Sweden), not being possible to identify any compositional pattern. This alteration can be related to the commercialisation of glass paints and the industrial production of new formulations [3]. The LIBS results (Table 3), allowed the identification of boron in two of the grisailles studied, SS03 and UC3, from Germany and Sweden, respectively. This can prove what was proposed by Bettembourg [56] as the use of borax ($Na_2B_4O_7{\cdot}10H_2O$) to lower the melting temperature of the grisailles without needing high amounts of lead. However, in this case, it is possible to associate the presence of boron with higher quantities of zinc (2.44–5.32 wt. %), indicating the use of lead–zinc borosilicate glass as base glass instead of a lead-silica glass. [65] Lead–zinc borosilicate glass was previously identified in enamels studied by Beltrán et al. [65], pointing towards the replacement of the common rocaille (SiO_2: PbO 1:3) by an enamel glass as the base glass in the production of grisaille paints in these centuries.

By looking at their composition (Fig. 3) and their position on the ternary graph (Fig. 7), it was possible to propose a chronology for the two samples with unknown dates, LS02 and LS04. Both samples present higher quantities of manganese. In addition, sample LS04 also has a significant quantity of cobalt, indicating that both samples could be ascribed to 19th or 20th-century stained-glass productions.

Regarding the paint layers thickness, the results obtained (Table 4) did not facilitate to understand if the thickness variation is directly related to the chronology or provenance of the samples. There is a slight indication that the more modern samples, with chronologies from the nineteenth and twentieth centuries, generally present thinner and more homogeneous layers for their *grisailles à modeler*. This can be related to heavier industrialisation of the paints production, allowing for a better ground mixture, easy to apply, and a change in the painting style.

Methodology proof

With the multi-analytical and complementary approach applied throughout this study it was possible to obtain accurate chemical composition and layers thickness of the grisaille paints.

EDXRF and PIXE analysis allowed the identification of the chemical composition of both the glass substrate and painted layers. However, complemented with the LIBS and LIF results, a more in-depth information was obtained. The LIBS results showed a high sensitivity for

the characterisation of grisaille paint layers composition, being possible to distinguish key elements that could give information on the manufacture of this historical material. Even with a qualitative analysis, LIBS proves capable of detecting the presence of light and trace elements, as well as chromophores, highlighting differences in composition, not only on the grisaille layers but also on the support glasses. The advantage of this technique is that the pieces can be analysed in situ on the surface without needing a sample to be taken. The micro-ablation that occurs during the analysis can be interpreted as micro-destructive. Nevertheless, this ablation allows the cleaning of any surface layer of alteration and to analyse the material as close as the original. By contrary by EDXRF and PIXE, to ensure that the compositions obtained are the closest to the original ones and do not suffer from interferences of possible degradation layers, as we saw for the samples SS02 and SS04, a small piece needs to be taken and mounted in resin in order to be analysed in cross-section.

As mentioned previously, the results from the NLOM-MPEF showed good agreement with the measurements taken with the OM images. Following the study of Oujja et al. [40], this study validates this technique as an adequate non-destructive way to retrieve the thickness of this paint layers. Beyond the non-destructive characteristic, as the analysis is done on the surface without the need for sampling, NLOM also presents other advantages when applied to cultural heritage objects compared to confocal microscopes. The confocal microscopes have a higher risk of potentially damaging the analysed material and cannot penetrate deeply into materials. These issues are overcome with the femtosecond lasers used for the excitation of the MPEF signal. In this study, only the modality of MPEF of NLOM was tested. Nonetheless, SHG and THG could also be used to study grisaille layers to determine structural information of crystalline or highly organised structures without inversion symmetry (by SHG) and the boundaries and positions of layers (by THG) [15, 38, 39].

Conclusions

In this study, a multi-analytical and complementary approach was applied to characterise the grisaille paint layers and uncover the evolution of the manufacturing production of these heritage materials throughout time. The study has allowed to distinguish between different classifications of the support glasses used, verifying that the glass compositions usually correspond to the common ones found for the chronology and provenance of the samples. The multi-analytical approach for the grisaille paint layers allows for more accurate and complete composition identification. Compositional differences and patterns have been identified throughout the samples when comparing the results obtained with those from the literature. Between these patterns, it is noted the preference for the use of copper as a colouring agent in the Central and South-Central European countries, as seen in the samples from Poland (CG), and the addition of new compounds (CoO, Cr_2O_3, MnO) as colouring agents in the 19th and 20th-century samples. The LIBS analysis also allowed the identification of boron in two samples, SS03 and UC3, confirming that at one point, around the seventeenth century, the lead base glass of the grisailles started to be replaced by different compounds or glasses. However, it is still unclear under which circumstances this change happened as contemporary to that, it is also still possible to find grisailles with base glasses with high contents of lead. For the studied samples, as they also presented high amounts of zinc, with a similar composition to that of lead–zinc borosilicate enamels, it is possible to propose that an enamel glass could have been used instead of the common lead-silicate glass from the grisailles. With these analyses, it was also possible to identify misattributions of chronology on the samples and clarify if a specific dark paint on glass is a grisaille paint layer or a dark enamel.

The thickness of the grisailles was obtained, validating the NLOM-MPEF capability for the non-invasive measurement of the different paint layers from historic stained-glass windows. The results showed that promoted by the intrinsic heterogenic properties of the grisailles, a great variety of thickness is found, even across the same fragment.

To conclude, a multi-analytical and complementary approach is always the best option to achieve a better material characterisation. Nevertheless, it is also important to look for and test a non- or micro-destructive techniques when analysing historical materials, to better protect them and overcome restrictions on the sampling process.

Supplementary Information

The online version contains supplementary material available at https://doi.org/10.1186/s40494-023-00917-4.

Additional file 1: **Table S1.** Composition (wt. %) of the glass support of each sample as obtained by μ-EDXRF.

Acknowledgements

The authors wish to thank all that allow us access to samples to develop this study: Joost Caen (Antwerp University, Belgium) Elisabeth Sinnerud and Marie Louise Anker (Nidarosdomen, Norway), Linda Kvarnström and Emma Newman (Stained-Glass Studio, Uppsala Cathedral, Sweden), Marta Kaminska (Jan Matejko Academy of Fine Arts Krakow, Poland), Leonie Seliger (Restoration Atelier Canterbury, UK), to Glasmalerei Otto Peters (Germany) and to Pedro Redol (Batalha Monastery, Portugal). The authors are also grateful to Trinitat Pradell and Mingyue Yuan (Universitat Politècnica de Catalunya, Spain) for the preparation of the samples and the optical microscopy analysis.

Author contributions

Conceptualization, TP, MO and MV; methodology, CM and MO; validation, TP, MO and LCA, investigation, CM MO, LCA, MMW, LMG, PMCQ, writing—original draft preparation, CM; writing—review and editing, CM, MO, LCA, MMW, LMG, PMCQ, MC, MV and TP; supervision, MC, MV, TP. All authors have read and agreed to the published version of the manuscript. All authors read and approved the final manuscript.

Funding
This research has been funded by the H2020 European project IPERION HS (Integrated Platform for the European Research Infrastructure ON Heritage Science, GA 871034), by the Spanish State Research Agency (AEI) through project PID2019-104124RB-I00/AEI/, by the Fundação de Ciência e Tecnologia de Portugal (project ref. UIDB/EAT/00729/2020, UIDP/00729/2020, LA/P/0008/2020, UIDB/ 04349/2020 and PTDC/ART-PER/1702/2021, researcher grant CEEC-IND/02249/2021 and doctoral grant ref. PD/BD/136673/2018) and by project TOP Heritage-CM (S2018/NMT-4372) from Community of Madrid.

Availability of data and materials
All data analysed during this study are available in digital.CSIC repository.

Competing interests
The authors declare no competing interests.

Author details
[1]Departmento de Conservação e Restauro, Nova School of Science and Technology, 2829-516 Caparica, Portugal. [2]VICARTE - Glass and Ceramics for the Arts, Nova School of Science and Technology, 2829-516 Caparica, Portugal. [3]Instituto de Quimica Fisica Rocasolano (IQFR), CSIC, 28006 Madrid, Spain. [4]Campus Tecnológico e Nuclear, IST,, Universidade de Lisboa, 2695-066 Bobadela, Portugal. [5]Instituto de Ceramica e Vidrio (ICV), CSIC, 28049 Madrid, Spain.

Received: 22 December 2022 Accepted: 25 March 2023
Published online: 27 April 2023

References

1. Machado C, Machado A, Palomar T, Vilarigues M. Grisaille in historical written sources. J Glass Stud. 2019;61:71–86.
2. Schalm O. Characterization of paint layers in stained-glass windows: main causes of the degradation of nineteenth century grisaille paint layers. [Antwerpen]: Universiteit Antwerpen. 2000.
3. Machado C, Vilarigues M, Palomar T. Historical grisailles characterisation: a literature review. J Cult Herit. 2021;49:239–49.
4. Hawthorne JG, Smith CS. Theophilus: On divers arts the foremost medieval treatise on painting, glassmaking and metalwork. New York: Dover Publications, INC; 1979.
5. Vilarigues M, Machado C, Machado A, Costa M, Alves LC, Cardoso IP, et al. Grisailles: reconstruction and characterization of historical recipes. Int J Appl Glas Sci. 2020;11:756–73.
6. Verità M. Composition, structure et Mécanisme de Détérioration des Grisailles. Doss la Comm R des Monum sites Fouill. 1996;3:61–8.
7. Spencer HM, Murdoch KR, Buckman J, Forster AM, Kennedy CJ. Compositional analysis by p-XRF and SEM–EDX of medieval window glass from Elgin Cathedral. Northern Scotland Archaeom. 2018;60:1018–35.
8. Silvestri A, Molin G, Pomero V. 2011 The stained glass window of the southern transept of St. Anthony's Basilica (Padova, Italy): Study of glasses and grisaille paint layers. Spectrochim Acta - Part B At Spectrosc. Elsevier B.V. 66:81–7.
9. Palomar T. Chemical composition and alteration processes of glasses from the Cathedral of León (Spain). Bol la Soc Esp Ceram y Vidr. 2018;57:101–11.
10. Cílová ZZ, Kučerová I, Knížová M, Trojek T. Corrosion damage and chemical composition o Czech stained glass from 13th to 15th century. Glas Technol Eur J Glas Sci Technol Part A. 2015;56:153–62.
11. Carmona N, Ortega-Feliu I, Gómez-Tubío B, Villegas MA. Advantages and disadvantages of PIXE/PIGE, XRF and EDX spectrometries applied to archaeometric characterisation of glasses. Mater Charact Elsevier. 2010;61:257–67.
12. Bollati R, Huber E, Prunas ME, Santopadre P, Verità M. The conservation of a fourteenth-century satined-glass window from Assisi, Italy. In: Shepard MB, Pilosi L, Strobl S, editors. Proc forum conserv restor stain glas art collab stain conserv twenty-first century new york city, June 1–3 2009. London: Harvey Miller; 2010. p. 161–8.
13. Pradell T, Molina G, Murcia S, Ibáñez R, Liu C, Molera J, et al. Materials, techniques and conservation of historic stained glass "grisailles." Int J Appl Glas Sci. 2016;7:41–58.
14. Palomar T, Grazia C, Pombo Cardoso I, Vilarigues M, Miliani C, Romani A. Analysis of chromophores in stained-glass windows using Visible Hyperspectral Imaging in-situ. Spectrochim Acta Part A Mol Biomol Spectrosc Elsevier. 2019;223:117378.
15. Filippidis G, Massaouti M, Selimis A, Gualda EJ, Manceau J-M, Tzortzakis S. Non-linear imaging and THz diagnostic tools in the service of Cultural Heritage. Appl Phys A. 2012;106:257–63.
16. Rahrig M, Torge M. 3D Inspection of the Restoration and Conservation of Stained Glass Windows using High Resolution Structured Light Scanning. Int Arch Photogramm Remote Sens Spat Inf Sci—ISPRS Arch. Hanover, Germany: International Society of Photogrammetry and Remote Sensing (ISPRS). 2019. 965–72.
17. Oujja M, Sanz M, Agua F, Conde JF, García-Heras M, Dávila A, et al. Multianalytical characterization of late roman glasses including nanosecond and femtosecond laser induced breakdown spectroscopy. J Anal At Spectrom. 2015;30:1590–9.
18. Palomar T, Oujja M, García-Heras M, Villegas MA, Castillejo M. Laser induced breakdown spectroscopy for analysis and characterization of degradation pathologies of Roman glasses. Spectrochim Acta—Part B At Spectrosc. 2013;87:114–20.
19. Muller K, Stege H. Evaluation of the analytical potential of laser-induced breakdown spectrometry (LIBS) for the analysis of historical glasses. Archaeometry. 2003;45:421–33.
20. Carmona N, Oujja M, Rebollar E, Römich H, Castillejo M. Analysis of corroded glasses by laser induced breakdown spectroscopy. Spectrochim Acta Part B At Spectrosc. 2005;60:1155–62.
21. Klein S, Stratoudaki T, Zafiropulos V, Hildenhagen J, Dickmann K, Lehmkuhl T. Laser-induced breakdown spectroscopy for on-line control of laser cleaning of sandstone and stained glass. Appl Phys A Mater Sci Process. 1999;69:441–4.
22. Gerhard C, Hermann J, Mercadier L, Loewenthal L, Axente E, Luculescu CR, et al. Quantitative analyses of glass via laser-induced breakdown spectroscopy in argon. Spectrochim Acta Part B At Spectrosc Elsevier. 2014;101:32–45.
23. Negre E, Motto-Ros V, Pelascini F, Lauper S, Denis D, Yu J. On the performance of laser-induced breakdown spectroscopy for quantitative analysis of minor and trace elements in glass. J Anal At Spectrom. 2015;30:417–25.
24. Carmona N, Oujja M, Gaspard S, García-Heras M, Villegas MA, Castillejo M. Lead determination in glasses by laser-induced breakdown spectroscopy. Spectrochim Acta Part B At Spectrosc. 2007;62:94–100.
25. Palomar T, Martínez-Weinbaum M, Aparicio M, Maestro-Guijarro L, Castillejo M, Oujja M. Spectroscopic and microscopic characterization of flashed glasses from stained glass windows. Appl Sci. 2022;12:5760.
26. Melessanaki K, Mateo M, Ferrence SC, Betancourt PP, Anglos D. The application of LIBS for the analysis of archaeological ceramic and metal artifacts. Appl Surf Sci. 2002;197–198:156–63.
27. Giakoumaki A, Melessanaki K, Anglos D. Laser-induced breakdown spectroscopy (LIBS) in archaeological science-applications and prospects. Anal Bioanal Chem. 2007;387:749–60.
28. Martínez-Hernández A, Oujja M, Sanz M, Carrasco E, Detalle V, Castillejo M. Analysis of heritage stones and model wall paintings by pulsed laser excitation of Raman, laser-induced fluorescence and laser-induced breakdown spectroscopy signals with a hybrid system. J Cult Herit Elsevier Masson SAS. 2018;32:1–8.
29. Ehrt D. Photoluminescence in glasses and glass ceramics. IOP Conf Ser Mater Sci Eng. 2009;2: 012001.
30. Fournier J, Néauport J, Grua P, Jubera V, Fargin E, Talaga D, et al. Luminescence study of defects in silica glasses under near-UV excitation. Phys Procedia Elsevier. 2010;8:39–43.
31. Reisfeld R, Boehm L, Barnett B. Luminescence and nonradiative of Pb2+, Sn2+, Sb3+, and Bi3+ in Oxide Glasses. J Solid State Chem. 1975;15:140–50.
32. Reisfeld R. Inorganic ions in glasses and polycrystalline pellets as fluorescence standard reference materials. J Res Natl Bur Stand Sect A Phys Chem. 1972;76A:613.
33. Filippidis G, Tserevelakis GJ, Selimis A, Fotakis C. Non-linear imaging techniques as non-destructive high-resolution diagnostic tools for cultural heritage studies. Appl Phys A Mater Sci Process. 2014;118:417–23.
34. Oujja M, Psilodimitrakopoulos S, Carrasco E, Sanz M, Philippidis A, Selimis A, et al. Non-linear imaging microscopy for assessing structural and photochemical modifications upon laser removal of dammar varnish on photosensitive substrates. Phys Chem Chem Phys. 2017;19:22836–43.
35. Villafana TE, Brown WP, Delaney JK, Palmer M, Warren WS, Fischer MC. Femtosecond pump-probe microscopy generates virtual cross-sections in historic artwork. Proc Natl Acad Sci. 2014;111:1708–13.

36. Dal Fovo A, Sanz M, Mattana S, Oujja M, Marchetti M, Pavone FS, et al. Safe limits for the application of non-linear optical microscopies to cultural heritage: a new method for in-situ assessment. Microchem J Elsevier. 2020;154:104568.
37. Dal Fovo A, Sanz M, Oujja M, Fontana R, Mattana S, Cicchi R, et al. In-depth analysis of egg-tempera paint layers by multiphoton excitation fluorescence microscopy. Sustainability. 2020;12:1–15.
38. Latour G, Echard J-P, Didier M, Schanne-Klein M-C. In situ 3D characterization of historical coatings and wood using multimodal non-linear optical microscopy. Opt Express. 2012;20:24623.
39. Chen Y-C, Hsu H-C, Lee C-M, Sun C-K. Third-harmonic generation susceptibility spectroscopy in free fatty acids. J Biomed Opt. 2015;20: 095013.
40. Oujja M, Agua F, Sanz M, Morales-Martin D, García-Heras M, Villegas MA, et al. Multiphoton excitation fluorescence microscopy and spectroscopic multianalytical approach for characterization of historical glass grisailles. Talanta Elsevier. 2021;230:122314.
41. Canberra, UA-MiTAC. WinAxil Software Package—Brief Installation and Operational Guide, MAnual Version 1.5. Zellik, Belgium Canberra Eurisys Benelux. 2003.
42. Louro S. O vitral e as suas tintas: Grisalha e Amarelo de Prata. Master dissertation NOVA University of Lisbon. 2017.
43. Delgado J. Vitrais da charola do Convento de Cristo em Tomar. História e Caracterização. Faculdade de Ciências e Tecnologias: Universidade Nova de Lisboa; 2010.
44. Schalm O, Janssens K, Wouters H, Caluwé D. Composition of 12–18th century window glass in Belgium: non-figurative windows in secular buildings and stained-glass windows in religious buildings. Spectrochim Acta - Part B. 2007;62:663–8.
45. Dungworth D. The value of historic window glass. Hist Environ Policy Pract. 2011;2:21–48.
46. Rodrigues A. The glass collection of Ferdinand II in Museu Nacional de Arte Antiga study and preservation. Nova Univerty of Lisbon—Faculty of Science and Technology. 2018.
47. Vilarigues M, Delgado J, Redol P. Stained glass from the convent of Christ in tomar Portugal history and characterization. J Glass Stud. 2011;53:246–51.
48. Caen J. The Production of stained glass in the country of Flanders and Duchy of Brabant from the XVth to the XVIIIth centuries: Materials and Techniques. Antwerp: Brepols; 2009.
49. NIST atomic spectra database online. Available from. https://www.nist.gov/pml/atomic-spectra-database. Date of Access: Feb. 2022
50. Brill RH. The scientific investigation of ancient glass. In: Charleston RJ, Evans W, Werner AE, editors. Stud glas hist desviiith int congr glas. London: Society of Glass Technology; 1968. p. 47–68.
51. Brill RH. Scientific studies of stained glass: a progress report. J Glass Stud. 1970;12:185–92.
52. El Vidrio NJ. 3rd Editio. Madrid: CSIC Universitarios; 2003.
53. Delgado J, Vilarigues M, Ruivo A, Corregidor V, Silva RC, Alves LC. Characterisation of medieval yellow silver stained glass from convento de cristo in tomar, Portugal nucl instruments methods Phys res sect b beam interact with mater atoms. Elsevier. 2011;269:2383–8.
54. Machado C, Vilarigues M, Palomar T. Characterization of the alteration of debitus grisailles. Stud Conserv Routledge. 2022;67:413–22.
55. Verità M. Paintwork in medieval stained-glass windows: composition, weathering, and conservation. In: Shepard MB, Pilosi L, Stroble S, editors. Proc forum conserv restor stain glas art collab stain conserv twenty-first Century New York City June 1–3 2009. London: Harvey Miller; 2010. p. 210–6.
56. Bettembourg J-M. Composition er durabilité des grisailles. Sci Technol la Conserv la Restaur des oeuvres d'art du Patrim. 1991;2:47–55.
57. Beltran M, Schibille N, Gratuze B, Vallcorba O, Bonet J, Pradell T. Composition, microstructure and corrosion mechanisms of Catalan modernist enamelled glass. J Eur Ceram Soc Elsevier Ltd. 2021;41:1707–19.
58. García-Heras M, Carmona N, Gil C, Villegas MA. Neorenaissance/neobaroque stained glass windows from madrid: a characterisation study on some panels signed by the Maumejean Fréres company. J Cult Herit. 2005;6:91–8.
59. Vilarigues M, Fernandes P, Alves LC, da Silva RC. Stained glasses under the nuclear microprobe: a window into history. Nucl Instruments Methods Phys Res Elsevier. 2009;267:2260–4.
60. Kunckel J. Ars Vitraria Experimentalis. Frankfurt/Leipzig. 1679.
61. Marschner H. Analyses de pigments de grisaille sur des vitraux munichois de L'Église du Saint-Sauveur, Réalisés vers 1500. Doss la Comm R des Monum sites Fouill. 1996;3:53–9.
62. Machado A. Historical stained glass painting techniques—technology and preservation NOVA University of Lisbon. Lisbon: Faculty of Sciences and Technology; 2018.
63. Volf MB. Chemical Approach to Glass. 2nd ed. Utah: Igneous Glassworks; 1984.
64. Scholze H. Glass: nature, structure, and properties. New York: Springer International Publishing; 1991.
65. Beltrán M, Schibille N, Brock F, Gratuze B, Vallcorba O, Pradell T. Modernist enamels: composition microstructure and stability. J Eur Ceram Soc. 2020;40:1753–66.
66. Skuja L. Optically active oxygen-deficiency-related centers in amorphous silicon dioxide. J Non Cryst Solids. 1998;239:16–48.
67. Stevens-Kalceff MA. Cathodoluminescence microcharacterization of point defects in α-quartz. Mineral Mag. 2009;73:585–605.
68. Reisfeld R, Lieblich N. Absorption and fluorescence of lead in germanate, borate and phosphate glasses. J Non Cryst Solids. 1973;12:207–12.
69. Schultz PC. Optical absorption of the transition elements in vitreous silica. J Am Ceram Soc. 1974;57:309–13.
70. Fovo AD, Oujja M, Sanz M, Martínez-Hernández A, Cañamares MV, Castillejo M, et al. Multianalytical non-invasive characterization of phthalocyanine acrylic paints through spectroscopic and non-linear optical techniques. *Spectrochim* acta—part a mol biomol spectrosc. Elsevier. 2019;208:262–70.
71. White GW. Improving the accuracy of vertical measurments under the microscope. Microscope. 1970;18:51–9.
72. Rodrigues A, Coutinho ML, Machado C, Alves LC, Machado A, Vilarigues M. An Overview of germanic grisailles through the stained-glass collection at pena palace. Heritage. 2022;5:1003–23.
73. Verità M, Nicola C, Sommariva G. The stained glass windows of the Sainte Chapelle in Paris: Investigations on the origin of the loss of the painted work. AIHV Ann du 16 Congrès. 2003. 347–51.
74. Rodrigues A, Machado C, Coutinho M, Machado A, Vilarigues M. Chemical chracterisation of the Low Coutries 16th and 17th-century grisailles from Pena Palace collection. 22nd Int Congr Assoc Int pour l'Histoire du Verre, Lisbon. 2022. press.
75. Fernandes P, Vilarigues M, Alves LC, da Silva RC. Stained glasses from monastery of Batalha: non-destructive characterisation of glasses and glass paintings. J Cult Herit. 2008;9:e5-9.
76. Van der Snickt G, Schalm O, Caen J, Janssens K, Schreiner M. Blue enamel on sixteenth—and seventeenth-century window glass. Stud Conserv. 2006;51:212–22.
77. Machado A, Wolf S, Alves LC, Katona-Serneels I, Serneels V, Trümpler S, et al. Swiss stained-glass panels: an analytical study. Microsc Microanal. 2017;23:878–90.

Publisher's Note